FORMULATION OF SPECTRAL TRUSS ELEMENT FOR GUIDED WAVES DAMAGE DETECTION IN SPATIAL STEEL TRUSSES

J. CHRÓŚCIELEWSKI[1], M. RUCKA[2], K. WILDE[3], W. WITKOWSKI[4]

This study presents a spectral finite element and time integration scheme for wave propagation in spatial truss structures of arbitrary geometry. The current approach does not limit the number of nodes per element. The numerical simulations have been performed for an ideal truss as well as for the truss with singularity points imposed by the additional mass. The accelerations time histories of elastic waves have been applied to find the locations of the additional masses. The detection of truss singularities based on the analysis of elastic waves is discussed.

Keywords: Elastic wave propagation, spectral element method, spatial truss, structural health monitoring.

1. I

Low amplitude elastic waves can be used for damage detection systems (e.g., [1, 2]). The travelling waves pass through the structure reflecting and refracting on the geometric boundaries, joints, cracks, internal flaws or some other irregularities. The information carried out by the waves can be decoded and the location of the damage can be found. Methods based on groups of waves induced simultaneously on the structure and having carefully selected properties are called guided wave techniques.

The study on very complex problem of elastic waves propagation in large structures is in relatively early stage. Modelling of wave propagation is possible using the finite element method (FEM) [3, 4]. However, the numerical integration becomes very time-consuming since wave propagation concerns high frequencies and the elements must be very fine (i.e. of order of wavelength). One of very effective techniques to

[1] Professor. Department of Structural Mechanics and Bridge Structures, Faculty of Civil and Environmental Engineering, Gdańsk University of Technology, Gdańsk, Poland, e-mail: jchrost@pg.gda.pl

[2] PhD. Department of Structural Mechanics and Bridge Structures, Faculty of Civil and Environmental Engineering, Gdańsk University of Technology, Gdańsk, Poland, e-mail: magdalena.rucka@wilis.pg.gda.pl

[3] DSc. Department of Structural Mechanics and Bridge Structures, Faculty of Civil and Environmental Engineering, Gdańsk University of Technology, Gdańsk, Poland, e-mail: krzysztof.wilde@wilis.pg.gda.pl

[4] PhD. Department of Structural Mechanics and Bridge Structures, Faculty of Civil and Environmental Engineering, Gdańsk University of Technology, Gdańsk, Poland, e-mail: wojciech.witkowski@wilis.pg.gda.pl

solve the wave propagation problems is the spectral finite element method (SFEM) developed by D [5]. This technique, based of Fourier spectral analysis, is in fact the finite element method formulated in the frequency domain. The analysis of wave propagation by the SFEM in the cracked rod, Timoshenko beam and plate can be found in references [6, 7, 8]. The FSEM has been widely extended by G *et al.* for anisotropic media [9].

P [10] in 1984 in the context of fluid dynamics developed a different approach called spectral element method (SEM). This method is an expansion of FEM. The main idea of the SEM is the using of one high-order polynomial for each domain. The spectral element method has the same view point as the *p*-version of the finite element method [11]. In the SEM the Lagrange polynomials are applied at the Gauss-Legendre-Lobbatto nodes [11]. The spectral elements are available for elementary elements. The wave propagation in rod, beam membrane and plate elements using SEM method were presented by K *et al.* [12] [13] and Ż *et al.* [14]. The shell element was presented by Ż *et al* [15]. However, there are very few studies on numerical models for the analysis of wave propagation in a truss structure in time domain.

This study presents a formulation of a spectral finite element and time integration scheme for wave propagation in spatial truss structures of arbitrary geometry. As the shape functions of a single truss element, the high order Lagrange interpolation polynomial is used. To integrate element matrices we use the Gauss-Lobatto-Legendre (GLL) quadrature rule with the appropriate distribution of the quadrature points. The formulation contains the details of the transformation of local quantities to a global frame of the structure. The derivation of temporal integration schemes of the Newmark type formulated in terms of displacements or in terms of acceleration (*a*-form) is presented. The time integration scheme is devoted to the problems concerning wave propagation in structures with complex geometry. The numerical simulations have been performed for an ideal truss of a shape of the star dome as well as for the truss with singularity points imposed by the additional mass.

2. F

The SEM element is viewed in this paper as C^0 isoparametric displacement finite element. The accuracy of the FEM results may be improved using one (or combination) of the following approaches: decreasing the element size keeping fixed the interpolation polynomial (known as *h*-refinement) and/or by increasing the order of polynomial remaining the size element fixed (known as *p*-refinement). The SEM is based on the *p*-refinement. This is due to the fact that the higher order polynomials used in such approach enable more accurate wave propagation simulations.

In addition, in the SEM approach the use is made of the GLL quadrature rule to integrate the element matrices. Consequently, and with proper distribution of element

nodes (this issue is discussed later in the text), the mass matrix of C^0 element in the local coordinate system has diagonal structure, cf. for instance [12]. Therefore, it is possible to formulate the temporal integration schemes in terms of accelerations with straightforward inversion of diagonal or nearly diagonal mass matrix. This is in contrast to majority of the temporal integration schemes in structural dynamics that use the generalized displacements as the primary variables. As a consequence the inverted stiffness matrix is in principle not diagonal so that matrix decomposition is time consuming.

The formulation of the spectral truss element follows the classical steps, briefly recapitulated below. The study is concerned with the geometrically linear analysis and linear elastic material is considered.

2.1. S

Consider a straight truss rod from Fig. 1 with given: A – cross-section area, L – length, E – modulus of elasticity and ρ – mass density. The strong form of initial-boundary value problem is

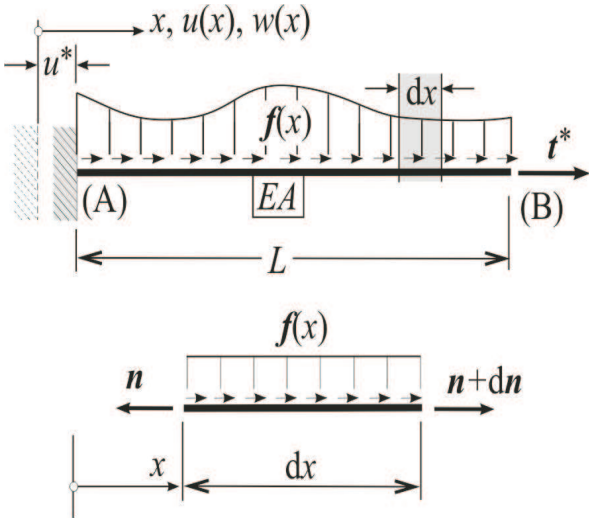

Fig. 1. Concept of truss element, local definitions.
Rys. 1. Element kratowy w układzie lokalnym

$$n_{,x} + f = \rho A\ddot{u} + cA\dot{u} \quad \text{on} \quad x \in [0; L], \qquad (.)_{,x} = d(.)/dx, \tag{2.1}$$

where n is the stress (axial force), f is the body force (that may include also damping effects),

$$u|_{x=0} = u^*, \quad n|_{x=L} = t^* \tag{2.2}$$

are Dirichlet and Neumman boundary conditions respectively and

$$u(x)|_{t=0} = u_0(x), \quad \dot{u}(x)|_{t=0} = v_0(x) \tag{2.3}$$

are the initial conditions. The superposed dot denotes time derivative and c is the damping density assumed to be positive. It is assumed that ρ and c are proportional (up to the units) $\eta = c/\rho$ where η denotes proportional damping coefficient.

The stress is understood as the function of displacement through the constitutive relation $n = EA\varepsilon$ in connection with the kinematical (virtual) relations

$$\varepsilon = u_{,x} \quad (\delta\varepsilon \equiv \delta u_{,x}). \tag{2.4}$$

Here $\delta u(x)$ denotes kinematically admissible virtual displacements. In the course of classical steps, the weak form (principle of virtual displacements) corresponding to (2.1) is obtained as

$$\begin{aligned} \delta W &\equiv \delta W_{\text{int}} + \delta W_{\text{kin}} + \delta W_{\text{damp}} - \delta W_{\text{ext}} \\ &= \int_L \delta\varepsilon EA\,\varepsilon \mathrm{d}x + \int_L \delta u \rho A\,\ddot{u}\mathrm{d}x + \int_L \delta u \eta A\,\dot{u}\mathrm{d}x - \int_L \delta u f\,\mathrm{d}x - \delta u\, t^* = 0. \end{aligned} \tag{2.5}$$

2.2. I ,

Let $\xi \in [-1, +1]$ is the natural coordinate of an element and N is the number of element nodes. The vector-type variables are interpolated in the way usual for C^0 isoparametric elements way (e.g. [19]) i.e.

$$\tilde{z}(\xi) = \sum_{i=1}^{N} L_i^N(\xi) z_i = \mathbf{L}^{(e)}(\xi)\,\mathbf{z}^{(e)}, \tag{2.6}$$

where

$$\mathbf{z}^{(e)} = [z_1, z_2, ..., z_N]^T, \quad \mathbf{L}^{(e)}(\xi) = \left[L_1^N(\xi), L_2^N(\xi), ..., L_N^N(\xi)\right]. \tag{2.7}$$

Here $\mathbf{L}^{(e)}(\xi)$ is the shape function matrix of an element, $L_i^N(\xi)$ are the Lagrange interpolation polynomials of order $N-1$ that obey rules

$$L_i^N(\xi) = \prod_{k=1, k\neq i}^{N} \frac{\xi - \xi_k}{\xi_i - \xi_k}, \quad L_i^N\left(\xi_j\right) = \delta_{ij}, \quad \sum_{i=1}^{N} L_i^N(\xi) = 1, \tag{2.8}$$

where δ_{ij} is the Kronecker delta. Here $\mathbf{z}^{(e)}$ stands for vector of (any) nodal values of function $z_i = z(\xi_i)$ in element. In Eq. (2.6) $\tilde{z}(\xi)$ denotes the approximated values of: geometry $\tilde{x}(\xi)$, displacement field $\tilde{u}(\xi, t)$, virtual displacement field $\delta\tilde{u}(\xi)$. The same scheme (2.6) is used to interpolate the time derivatives of $u(\xi, t)$ i.e. acceleration $\ddot{u}(\xi, t)$ and velocity $\dot{u}(\xi, t)$.

The strains $\tilde{\varepsilon}(\xi, t)$ and virtual strains $\delta\tilde{\varepsilon}(\xi)$ are interpolated using standard relations

$$\tilde{\varepsilon}(\xi, t) = \sum_{i=1}^{N} B_i(\xi) u_i(t) = \mathbf{B}^{(e)}(\xi)\,\mathbf{u}(t)^{(e)}, \tag{2.9}$$

$$\delta\tilde{\varepsilon}(\xi) = \sum_{i=1}^{N} B_i(\xi)\delta u_i = \mathbf{B}^{(e)}(\xi)\,\delta\mathbf{u}^{(e)}. \tag{2.10}$$

The element strain-displacement operator $\mathbf{B}^{(e)}(\xi)$

$$\mathbf{B}^{(e)}(\xi) = [B_1(\xi), B_2(\xi), ..., B_N(\xi)] \tag{2.11}$$

is defined in terms of nodal quantities

$$B_i(\xi) = \frac{dL_i^N(\xi)}{d\xi} J(\xi)^{-1}, \quad J(\xi) = \sum_{j=1}^{N} \frac{dL_j^N(\xi)}{d\xi}\, x_j \tag{2.12}$$

and

$$\mathbf{u}^{(e)}(t) = [u_1(t), u_2(t), \ldots, u_N(t)]^T, \quad \delta\mathbf{u}^{(e)} = [\delta u_1, \delta u_2, \ldots, \delta u_N]^T \tag{2.13}$$

are the element displacement vector and virtual displacement vector. Taking into account (2.9) and (2.10) in equation (2.5) and skipping the time argument yields

$$\begin{aligned}\delta W_{\text{int}} &= (\delta\mathbf{u}^{(e)})^T \left(\int_L (\mathbf{B}^{(e)}(\xi))^T E^{(e)} A^{(e)}\, \mathbf{B}^{(e)}(\xi)\, \mathrm{d}x \right) \mathbf{u}^{(e)} \\ &= (\delta\mathbf{u}^{(e)})^T \mathbf{K}^{(e)} \mathbf{u}^{(e)} = (\delta\mathbf{u}^{(e)})^T \mathbf{r}^{(e)},\end{aligned} \tag{2.14}$$

$$\delta W_{\text{kin}} = (\delta\mathbf{u}^{(e)})^T \left(\int_L (\mathbf{L}^{(e)}(\xi))^T \rho^{(e)} A^{(e)}\, \mathbf{L}^{(e)}(\xi)\, \mathrm{d}x \right) \ddot{\mathbf{u}}^{(e)} = (\delta\mathbf{u}^{(e)})^T \mathbf{M}^{(e)} \ddot{\mathbf{u}}^{(e)}, \tag{2.15}$$

$$\delta W_{\text{damp}} = (\delta\mathbf{u}^{(e)})^T \left(\int_L (\mathbf{L}^{(e)}(\xi))^T c^{(e)} A^{(e)}\, \mathbf{L}^{(e)}(\xi)\, \mathrm{d}x \right) \dot{\mathbf{u}}^{(e)} = (\delta\mathbf{u}^{(e)})^T \mathbf{C}^{(e)} \dot{\mathbf{u}}^{(e)}, \tag{2.16}$$

$$\delta W_{\text{ext}} = (\delta \mathbf{u}^{(e)})^T \left(\int_L (\mathbf{L}^{(e)}(\xi))^T f^{(e)}(\xi)\, \mathrm{d}x \right) + \delta u_1 t_1^* + \delta u_N t_N^* = (\delta \mathbf{u}^{(e)})^T (\mathbf{f}_{\text{ext}}^{(e)} + \mathbf{f}_{\text{nod}}^{(e)}) = (\delta \mathbf{u}^{(e)})^T \mathbf{f}^{(e)}, \tag{2.17}$$

where $\underset{N\times 1}{\mathbf{r}^{(e)}}$ is the vector of internal forces, $\underset{N\times N}{\mathbf{K}^{(e)}}$ is the local stiffness matrix, $\underset{N\times N}{\mathbf{M}^{(e)}}$ is local mass matrix, $\underset{N\times N}{\mathbf{C}^{(e)}}$ is local damping matrix, $\underset{N\times 1}{\mathbf{f}^{(e)}} = \mathbf{f}_{\text{ext}}^{(e)} + \mathbf{f}_{\text{nod}}^{(e)}$ is the load vector composed of $\underset{N\times 1}{\mathbf{f}_{\text{ext}}^{(e)}} = \left\{ \int_{L^{(e)}} L_i f^{(e)} \mathrm{d}x \right\}$ – the vector of element applied forces per unit length and $\underset{N\times 1}{\mathbf{f}_{\text{ext}}^{(e)}} = \{t_1^*, 0, ..., 0, t_N^*\}^T$ – the vector of prescribed nodal forces.

2.3. N

To evaluate the element matrices the numerical integration is employed. Therefore, the formulae for the stiffness matrix, mass matrix and load vector become

$$\mathbf{K}^{(e)} \to K_{ij}^{(e)} = EA \sum_{p=1}^{M} B_i\left(\xi_p\right) B_j\left(\xi_p\right) w_p J\left(\xi_p\right), \tag{2.18}$$

$$\mathbf{M}^{(e)} \to M_{ij}^{(e)} = \rho A \sum_{p=1}^{M} L_i^N\left(\xi_p\right) L_j^N\left(\xi_p\right) w_p J\left(\xi_p\right), \tag{2.19}$$

$$\mathbf{f}_{\text{ext}}^{(e)} \to f_i^{(e)} = \sum_{p=1}^{M} L_i^N\left(\xi_p\right) f\left(\xi_p\right) w_p J\left(\xi_p\right), \tag{2.20}$$

where M is the number of integration points of the selected integration rule, $p \in 1, 2, ..., M$ is the label of ξ_p i.e. the abscissa and w_p is the corresponding weight.

In this paper the Gauss-Lobatto-Legendre (cf. for example [11]) quadrature rule will be used. Here the abscissas are obtained as the roots of the equation

$$\left(1 - \xi^2\right) \frac{dP^{M-1}(\xi)}{d\xi} = 0, \tag{2.21}$$

where P^M denotes the M–th order Legendre polynomial (see for instance [11])

$$P^M(\xi) = \frac{1}{2^M M!} \frac{d^M}{d\xi^M} \left[(\xi^2 - 1)^M \right]. \tag{2.22}$$

The weights w_p are found from

$$w_p = \frac{2}{M\,(M-1)\left(P^{M-1}\left(\xi_p\right)\right)^2}. \tag{2.23}$$

The roots of (2.21) are found numerically using Newton type procedures originally elaborated in Matlab by Greg von Winckel, downloadable from [16]. Other algorithms may found in [11] or [17] (for Gauss quadrature).

Based on Greg von Winckel's experience we have developed own Fortran procedures for finding roots ξ_p and associated weights w_p of the GLL quadrature of arbitrary large order. Following Greg von Winckel we have assumed the convergence criterion of order E^{-16} defined as the maximal absolute difference between ith and $(i-1)$th approximation of the root.

It should be stressed that due to the costs of computations, in our implementation equations (2.21) and (2.23) are not solved for each element. Instead, given the known number of nodes per elements for $N \leq 101$ the above calculations are carried out once at the beginning of the simulation. In our implementation, the computed values are stored in a common and are available for each element and at each time step. For $N > 101$, in order to avoid time-consuming calculations, we have created a library of the abscissas ξ_p and the weights w_p, stored in the external memory in a binary form. The values required in given calculations are uploaded once in the beginning from the external database.

The mass matrix of an element will be diagonal if integration points ξ_p in (2.19) are nodes ξ_i of the Lagrange interpolation polynomials in the natural coordinate system $\xi \in [-1,+1]$ (2.6) (2.7), which follows from (2.8). Then $M = N$ and as a consequence the formula (2.19) becomes

$$\mathbf{M}^{(e)} \to M_{pp}^{(e)} = \rho A \sum_{p=1}^{N} w_p J\left(\xi_p\right), \quad M_{ij}^{(e)} = 0, \quad i \neq j. \tag{2.24}$$

It should be stressed that here the coordinates of the interpolation nodes follow from distribution of the integration points that are not uniformly distributed in the natural domain as in standard isoparametric formulation (Fig. 2).

The above discussion shows why the Gauss-Legendre-Lobatto rule is used instead of standard Gauss quadrature. The latter can not be applied here due to the fact that it does not include the end nodes of an element. Hence the required inter-element continuity conditions can not be satisfied. Moreover, the distribution of nodes compatible with integration points of the GLL quadrature rule (the GLL nodes) eliminates the so-called the Runge oscillation effect appearing when the uniformly distributed nodes are used. Figure 2 shows the interpolation polynomial for 11-node element in two variants: the uniformly distributed (UD) nodes and the GLL nodes. In the first case, the Runge oscillation effect can be observed. The oscillations occur near the ends and

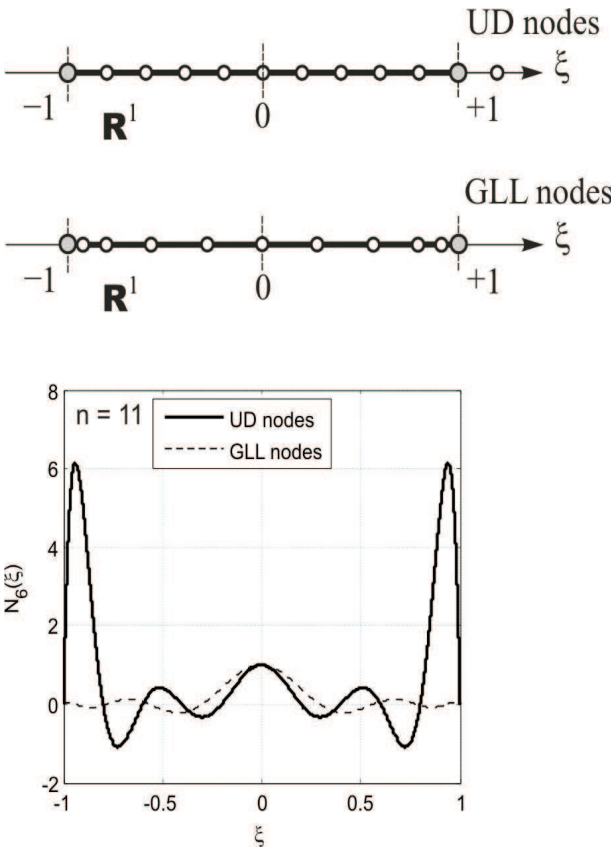

Fig. 2. Lagrange interpolation polynomial for GLL and UD distribution of nodes.
Rys. 2. Wielomian interpolacyjny Lagrange'a dla rozkładu węzłów typu GLL i węzłów równomiernie rozłożonych

they rise with the increase of the number of interpolation nodes. The Runge effect may lead to no reliable solution. This effect does not appear when the GLL nodes are used. Additionally, the mass matrix for the uniformly distributed nodes is significantly worse conditioned for the polynomial orders higher than 5 [18].

The above developments are generally well-known and therefore the discussion has been confined to necessary details. The most important aspects of the present formulation are covered in-depth in the following sections.

2.4. T

In the present paper the principal focus is on spatial trusses. Therefore, the transformation of local element matrices and vectors appears in the standard FEM approach. In comparison with the existing elements (see for instance [12]) the crucial point of our

formulation, is to devise transformation that will not cause the singularity associated with the internal nodes of the multi-node spectral truss element. The transformation is described as follows.

The structure is divided into spectral truss elements as illustrated in Fig. 3. Within an element there are two types of nodes distinguished: two external nodes $(1, N)$ with three structural degrees of freedom at each end of the element, and $(N-2)$ internal nodes $(2, 3, ..., N-1)$ with one degree of freedom along the element axis. According to hypothesis of truss element it is assumed that an element may experience only an overall rotation described by structural displacements of its end nodes so the element does not undergo bending and remains straight during the whole deformation. Simultaneously it can undergo elongation or shortening tangent to its (rotated) axis due to the displacements of the internal nodes. When the local axes of a finite element are not parallel to the structural axes, transformation from the local to structural axes must be performed.

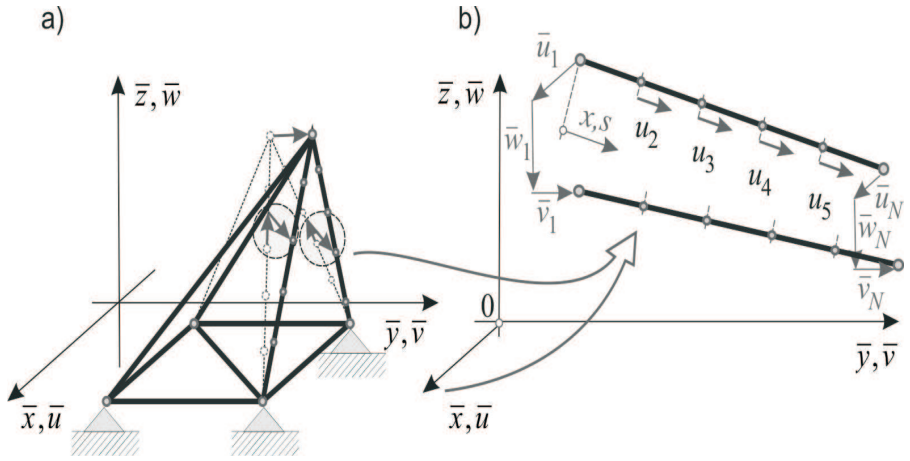

Fig. 3. Example of spatial truss structure modelled by SEM: a) overall spatial motion, b) nodal displacements definitions.
Rys. 3. Przykład kratownicy przestrzennej modelowanej elementami spektralnymi: a) ogólny ruch przestrzenny, b) definicja przemieszczeń węzłowych

Bearing in mind the effectiveness of the ultimate algorithm it is assumed that end nodes are transformed to the structural coordinate system while the internal nodes remain in the local frame. This eliminates additionally time-consuming transformations of the internal element nodes, which appear in the standard FEM approach. As a consequence, the final system of equations is of global-local character. Thus, in the considered N–node truss element the structural displacement $\mathbf{q}^{(e)}$ vector has $N+4$

components whereas the local nodal displacements vector $\mathbf{u}^{(e)}$ has N components

$$\mathbf{u}^{(e)} = [u_1, u_2, ..., u_N]^T,\ \mathbf{q}^{(e)} = [\mathbf{q}_1^T, u_2, ..., u_{N-1}, \mathbf{q}_N^T]^T,\ \mathbf{q}_i = \left\{ \begin{array}{c} \bar{u}_i \\ \bar{v}_i \\ \bar{w}_i \end{array} \right\},\ i = 1, N. \tag{2.25}$$

The local displacements $u_i, i = 1, N$, at each end of the element can be expressed by the structural displacements:

$$\mathbf{q}_i : \mathbf{t}_x \rightarrow u_i, \quad u_i = \mathbf{t}_x^T \mathbf{q}_i, \quad \mathbf{t}_x = \left\{ \begin{array}{c} \cos\alpha_{x\bar{x}} \\ \cos\alpha_{x\bar{y}} \\ \cos\alpha_{x\bar{z}} \end{array} \right\}, \quad i = 1, N, \tag{2.26}$$

where $\mathbf{t}_x$ is a unit vector of element axis composed of directional cosines $\cos\alpha_{x\bar{x}}$, $\cos\alpha_{x\bar{y}}$, $\cos\alpha_{x\bar{z}}$. Therefore, the transformation matrix $\mathbf{T}^{(e)}$ enabling the rotation of the local axes to the structural axes is given by

$$\mathbf{u}^{(e)} = \mathbf{T}^{(e)}\mathbf{q}^{(e)},\ \mathbf{T}^{(e)} = \left[\begin{array}{ccc} \mathbf{t}_x^T & 0 & 0 \\ 0 & \mathbf{1} & 0 \\ 0 & 0 & \mathbf{t}_x^T \end{array} \right]_{N\times(N+4)},\ \mathbf{1} = \left[\begin{array}{ccc} 1 & 0 & 0 \\ 0 & \ddots & 0 \\ 0 & 0 & 1 \end{array} \right]_{(N-2)\times(N-2)}. \tag{2.27}$$

The transformation of the local element stiffness matrix (2.18), the element load vector (2.20) and the vector of internal forces (2.17) to the structural coordinate system is then

$$\bar{\mathbf{K}}^{(e)} = \mathbf{T}^{(e)T}\mathbf{K}^{(e)}\mathbf{T}^{(e)}, \quad \bar{\mathbf{f}}^{(e)} = \mathbf{T}^{(e)T}\mathbf{f}^{(e)}, \quad \bar{\mathbf{r}}^{(e)} = \mathbf{T}^{(e)T}\mathbf{r}^{(e)}. \tag{2.28}$$

The inertia forces and mass matrix must take into account spatial motion of a structure. Therefore, in contrast to stiffness matrix, all three local nodal translational degrees of freedom $\mathbf{d}^{(e)}$ must be taken into account in the local mass matrix. Thus, in the case of the N–node truss element, the structural displacement vector $\mathbf{q}^{(e)}$ remains unchanged and has $N+4$ components, whereas the local nodal displacement vector $\mathbf{d}^{(e)}$ coupled with the inertia forces and mass matrix must be extended to $3N$ components

$$\mathbf{d}^{(e)} = [\mathbf{u}_1^T, \mathbf{u}_2^T, ..., \mathbf{u}_N^T]^T, \quad \mathbf{u}_i = \left\{ \begin{array}{c} u_i \\ v_i \\ w_i \end{array} \right\}, \quad i = 1, 2, 3, ..., N. \tag{2.29}$$

This follows from the fact that the transverse spatial motion of the truss element also generates inertia forces though such motion does not contribute to stiffness. Therefore, the local mass matrix $\mathbf{M}^{(e)}$ must be extended to accommodate all three

nodal degrees of freedom. It can be achieved either formally by appropriate direct approximation or by straightforward triple aggregation of $\mathbf{M}^{(e)}$ i.e.

(2.30)
$$\mathbf{M}^{(e)}_{N\times N} = [M^{(e)}_{ij}]_{N\times N} \rightarrow \hat{\mathbf{M}}^{(e)}_{3N\times 3N} = [\hat{\mathbf{m}}^{(e)}_{ij\,(3\times 3)}]_{N\times N},\ \hat{\mathbf{m}}^{(e)}_{ij} = \begin{bmatrix} M^{(e)}_{ij} & 0 & 0 \\ 0 & M^{(e)}_{ij} & 0 \\ 0 & 0 & M^{(e)}_{ij} \end{bmatrix}_{(3\times 3)}.$$

Thus, the element inertia force vector is

$$\hat{\mathbf{b}}^{(e)} = \hat{\mathbf{M}}^{(e)}\ddot{\mathbf{d}}^{(e)}. \tag{2.31}$$

However, $\mathbf{d}^{(e)}$ and its time derivatives must be subjected to the kinematical truss assumptions (constraints) discussed above. They can be elegantly introduced by making use of the dynamical generalized coordinates concept

$$\mathbf{d}^{(e)} = \mathbf{A}\mathbf{q}^{(e)}, \tag{2.32}$$

where the matrix $\mathbf{A}$ reads

(2.33)
$$\underset{3N\times(N+4)}{\mathbf{A}} = \begin{bmatrix} \mathbf{Q}^T & \mathbf{o} & \mathbf{o} & \cdots & \mathbf{o} & \mathbf{O} \\ \mathbf{o}^T & 1 & 0 & \cdots & 0 & \mathbf{o}^T \\ (1-\xi_2)\mathbf{t}_y^T & 0 & 0 & \cdots & 0 & \xi_2\mathbf{t}_y^T \\ (1-\xi_2)\mathbf{t}_z^T & 0 & 0 & \cdots & 0 & \xi_2\mathbf{t}_z^T \\ \mathbf{o}^T & 0 & 1 & \cdots & 0 & \mathbf{o}^T \\ (1-\xi_3)\mathbf{t}_y^T & 0 & 0 & \cdots & 0 & \xi_3\mathbf{t}_y^T \\ (1-\xi_3)\mathbf{t}_z^T & 0 & 0 & \cdots & 0 & \xi_3\mathbf{t}_z^T \\ \vdots & \vdots & \vdots & \ddots & \vdots & \vdots \\ \mathbf{o}^T & 0 & 0 & \cdots & 1 & \mathbf{o}^T \\ (1-\xi_{N-1})\mathbf{t}_y^T & 0 & 0 & \cdots & 0 & \xi_{N-1}\mathbf{t}_y^T \\ (1-\xi_{N-1})\mathbf{t}_z^T & 0 & 0 & \cdots & 0 & \xi_{N-1}\mathbf{t}_z^T \\ \mathbf{O}^T & \mathbf{o} & \mathbf{o} & \cdots & \mathbf{o} & \mathbf{Q}^T \end{bmatrix}, \underset{3\times 3}{\mathbf{O}} = \begin{bmatrix} 0 & 0 & 0 \\ 0 & 0 & 0 \\ 0 & 0 & 0 \end{bmatrix}, \underset{3\times 1}{\mathbf{o}} = \begin{Bmatrix} 0 \\ 0 \\ 0 \end{Bmatrix}$$

i.e. the end nodes ($i = 1, N$) undergo orthogonal transformation

$$\mathbf{u}_i = \mathbf{Q}^T\mathbf{q}_i, \mathbf{Q} = [\mathbf{t}_x \quad \mathbf{t}_y \quad \mathbf{t}_z], \mathbf{t}_x = \begin{Bmatrix} \cos\alpha_{x\bar{x}} \\ \cos\alpha_{x\bar{y}} \\ \cos\alpha_{x\bar{z}} \end{Bmatrix}, \mathbf{t}_y = \begin{Bmatrix} \cos\alpha_{y\bar{x}} \\ \cos\alpha_{y\bar{y}} \\ \cos\alpha_{y\bar{z}} \end{Bmatrix}, \mathbf{t}_z = \begin{Bmatrix} \cos\alpha_{z\bar{x}} \\ \cos\alpha_{z\bar{y}} \\ \cos\alpha_{z\bar{z}} \end{Bmatrix} \tag{2.34}$$

while the internal nodes ($i = 2, 3, ..., N-1$) are subjected to the constraints following from the assumption about rigid rotation

$$v_i = (1-\xi_i)\mathbf{t}_y^T\mathbf{q}_1 + \xi_i\mathbf{t}_y^T\mathbf{q}_N, \quad w_i = (1-\xi_i)\mathbf{t}_z^T\mathbf{q}_1 + \xi_i\mathbf{t}_z^T\mathbf{q}_N, \quad \xi_i = \frac{x_i}{l}. \tag{2.35}$$

The local mass element matrix $\hat{\mathbf{M}}^{(e)}$ and the element inertia force vector $\hat{\mathbf{b}}^{(e)}$ are transformed to the structural coordinate system by the matrix $\mathbf{A}^{(e)}$

$$\bar{\mathbf{M}}^{(e)} = \mathbf{A}^{(e)T}\hat{\mathbf{M}}^{(e)}\mathbf{A}^{(e)}, \quad \bar{\mathbf{b}}^{(e)} = \mathbf{A}^{(e)T}\hat{\mathbf{b}}^{(e)}. \tag{2.36}$$

Notations (2.27) and (2.36) are purely formal. In the implementation the extensive use is made of the fact that both $\mathbf{T}^{(e)}$ and $\mathbf{A}^{(e)}$ are sparse (pseudo-diagonal). The system of equation of motion is built in the course of standard aggregation of the element matrices and vectors referred to the structural coordinate system

$$\begin{gathered}\mathbf{M} = A_{e=1}^{N\_\{elem\}}\bar{\mathbf{M}}^{(e)}, \quad \mathbf{K} = A_{e=1}^{N\_\{elem\}}\bar{\mathbf{K}}^{(e)}, \quad \mathbf{r} = A_{e=1}^{N\_\{elem\}}\bar{\mathbf{r}}^{(e)}, \\ \mathbf{b} = A_{e=1}^{N\_\{elem\}}\bar{\mathbf{b}}^{(e)}, \quad \mathbf{p} = A_{e=1}^{N\_\{elem\}}\bar{\mathbf{f}}^{(e)}.\end{gathered} \tag{2.37}$$

The boundary conditions are introduced simultaneously with the aggregation process (2.37). The damping matrix and damping force vector are

$$\mathbf{C} = \eta\mathbf{M} + \alpha\mathbf{K}, \quad \mathbf{c} = \mathbf{C}\dot{\mathbf{q}}. \tag{2.38}$$

In the case of explicit time integration schemes it is required [19] that mass and damping matrices are diagonal for the method to be explicit. Therefore, (2.38) becomes

$$\alpha = 0 \;\Rightarrow\; \mathbf{C} = \eta\mathbf{M} \;\Rightarrow\; \mathbf{c} \to \{c_i\} = \eta\left\{b_i\dot{q}_i(\ddot{q}_i)^{-1}\right\}. \tag{2.39}$$

Thus, the final system of equation of motion and equilibrium condition are respectively

$$\mathbf{M}\ddot{\mathbf{q}} + \mathbf{C}\dot{\mathbf{q}} + \mathbf{K}\mathbf{q} = \mathbf{p}, \quad \mathbf{j} = \mathbf{p} - \mathbf{b}(\ddot{\mathbf{q}}) - \mathbf{c}(\dot{\mathbf{q}}) - \mathbf{r}(\mathbf{q}) = \mathbf{0}, \tag{2.40}$$

where $\mathbf{q}, \ddot{\mathbf{q}}$ and $\dot{\mathbf{q}}$ are structural vectors of displacements, accelerations and velocities, respectively.

In passing it should be noted that even if relation $\mathbf{M}^{(e)} \to \hat{\mathbf{M}}^{(e)}$ renders the diagonal matrix, as a consequence of the transformation (2.36) the element mass matrix referred to the structural coordinate system $\bar{\mathbf{M}}^{(e)}$ (2.37) is no longer diagonal. Nevertheless, this fact is concerned with end nodes only while the remaining part is diagonal. This fact is exploited in the implementation.

2.5. T

The temporal integration is performed in standard fashion. It is assumed that the solution of the linear equation of motion (2.40) is approximated $\mathbf{q}_n = \mathbf{q}(t_n)$ in finite number of time points $t_1, t_2, ..., t_n, ...$, and $\mathbf{q}_n, \dot{\mathbf{q}}_n$ and $\ddot{\mathbf{q}}_n$ are known from the previous step. Then we seek the solution at the next point $t_{n+1} = t_n + \Delta t$ writing $(2.40)_1$ as

$$\mathbf{M}\ddot{\mathbf{q}}_{n+1} + \mathbf{C}\dot{\mathbf{q}}_{n+1} + \mathbf{K}\mathbf{q}_{n+1} = \mathbf{p}_{n+1}, \tag{2.41}$$

where Δt is the time step. In the Newmark family [20] of the time integration schemes the solution at time instance t_{n+1} consists of the following approximations with respect to the accelerations $\ddot{\mathbf{q}}_{n+1}$ as the unknowns

$$\dot{\mathbf{q}}_{n+1} = \tilde{\mathbf{v}}_{n+1} + \Delta t\gamma\ddot{\mathbf{q}}_{n+1}, \qquad \tilde{\mathbf{v}}_{n+1} = \dot{\mathbf{q}}_n + \Delta t(1-\gamma)\ddot{\mathbf{q}}_n, \tag{2.42}$$

$$\mathbf{q}_{n+1} = \tilde{\mathbf{d}}_{n+1} + (\Delta t)^2\beta\ddot{\mathbf{q}}_{n+1}, \quad \tilde{\mathbf{d}}_{n+1} = \mathbf{q}_n + \Delta t\dot{\mathbf{q}}_n + \frac{1}{2}(\Delta t)^2(1-2\beta)\ddot{\mathbf{q}}_n. \tag{2.43}$$

The values of β and γ specify various integration schemes, cf. for instance [19]. These parameters are also responsible for the stability and the accuracy of the integration scheme. In the numerical simulations presented in the following Sections the trapezoidal rule is used with $\beta = 1/4$ and $\gamma = 1/2$.

Solving (2.43) with respect to $\ddot{\mathbf{q}}_{n+1}$ and substituting the result into (2.42) yields the relations

$$\dot{\mathbf{q}}_{n+1} = \underbrace{-\gamma(\Delta t\beta)^{-1}\mathbf{q}_n + (1-\gamma\beta^{-1})\dot{\mathbf{q}}_n + \Delta t(1-\frac{1}{2}\gamma\beta^{-1})\ddot{\mathbf{q}}_n}_{=\bar{\mathbf{v}}_{n+1}} + \gamma(\Delta t\beta)^{-1}\mathbf{q}_{n+1}, \tag{2.44}$$

$$\ddot{\mathbf{q}}_{n+1} = \underbrace{-(\Delta t)^{-2}\beta^{-1}[\mathbf{q}_n + \Delta t\dot{\mathbf{q}}_n + \frac{1}{2}(\Delta t)^2(1-2\beta)\ddot{\mathbf{q}}_n]}_{=\bar{\mathbf{a}}_{n+1}} + (\Delta t)^{-2}\beta^{-1}\mathbf{q}_{n+1}. \tag{2.45}$$

The temporal integration scheme proposed by authors is based on the pseudo-diagonal matrices $\mathbf{M}$ and $\mathbf{C}$. Combining (2.41) with (2.42) and (2.43) leads to the following equation with respect to the acceleration $\ddot{\mathbf{q}}_{n+1}$ as the unknown

$$\left[\mathbf{M} + \Delta t\gamma\mathbf{C} + (\Delta t)^2\beta\mathbf{K}\right]\ddot{\mathbf{q}}_{n+1} = \mathbf{p}_{n+1} - \mathbf{C}\tilde{\mathbf{v}}_{n+1} - \mathbf{K}\tilde{\mathbf{d}}_{n+1}, \ddot{\mathbf{q}}_{n+1} = \tilde{\mathbf{M}}^{-1}\left(\mathbf{p}_{n+1} - \tilde{\mathbf{j}}_{n+1}\right), \tag{2.46}$$

$$\tilde{\mathbf{M}} = \mathbf{M} + \Delta t\gamma\mathbf{C} + (\Delta t)^2\beta\mathbf{K}, \quad \tilde{\mathbf{j}}_{n+1} = \tilde{\mathbf{j}}_{n+1}(\mathbf{q}_n, \dot{\mathbf{q}}_n, \ddot{\mathbf{q}}_n) = \mathbf{C}\tilde{\mathbf{v}}_{n+1} + \mathbf{K}\tilde{\mathbf{d}}_{n+1}. \tag{2.47}$$

To obtain $\ddot{\mathbf{q}}_{n+1}$ it is necessary to find

$$\tilde{\mathbf{M}}^{-1} = [\mathbf{M} + \Delta t\gamma\mathbf{C} + (\Delta t)^2\beta\mathbf{K}]^{-1}. \tag{2.48}$$

For multi-node truss element the above formal inversion would be extremely time consuming. Yet, from (2.48) it is seen that if matrices $\mathbf{M}$ and $\mathbf{C}$ are pseudo-diagonal, as obtained from the GLL quadrature rule, a considerable reduction of computational time is obtained. Nevertheless, due to the fact that the stiffness matrix $\mathbf{K}$ is by definition

of full structure, the efficiency of the computation is limited. This problem may be overcome by rephrasing (2.41) in terms of the vectors of internal forces viz.

$$\mathbf{M}\ddot{\mathbf{q}}_{n+1} + \mathbf{C}\dot{\mathbf{q}}_{n+1} = \mathbf{p}_{n+1} - \mathbf{r}\left(\mathbf{q}_{n+1}\right). \tag{2.49}$$

Here $\mathbf{r}\left(\mathbf{q}_{n+1}\right)$ is found directly from (2.37), and therefore, the stiffness matrix $\mathbf{K}$ is not necessary. The present approach makes only sense with the pseudo-diagonal matrices $\mathbf{M}$ and $\mathbf{C}$, for the reasons discussed below.

Due to the presence of $\mathbf{q}_{n+1}$ on the right hand side of (2.49) the scheme is implicit, and therefore, requires iteration. By introducing iterative notation i.e.

$$\ddot{\mathbf{q}}_{n+1}^{(i+1)} = \ddot{\mathbf{q}}_{n+1}^{(i)} + \delta\ddot{\mathbf{q}}, \tag{2.50}$$

$$\dot{\mathbf{q}}_{n+1}^{(i+1)} = \underline{\dot{\mathbf{q}}_n + \Delta t[(1-\gamma)\ddot{\mathbf{q}}_n + \gamma\ddot{\mathbf{q}}_{n+1}^{(i)}]} + \Delta t\gamma\delta\ddot{\mathbf{q}} = \dot{\mathbf{q}}_{n+1}^{(i)} + \Delta t\gamma\delta\ddot{\mathbf{q}}, \tag{2.51}$$

$$\mathbf{q}_{n+1}^{(i+1)} = \underline{\mathbf{q}_n + \Delta t\dot{\mathbf{q}}_n + \frac{1}{2}(\Delta t)^2[(1-2\beta)\ddot{\mathbf{q}}_n + 2\beta\ddot{\mathbf{q}}_{n+1}^{(i)}]} + (\Delta t)^2\beta\delta\ddot{\mathbf{q}} = \ddot{\mathbf{q}}_{n+1}^{(i)} + (\Delta t)^2\beta\delta\ddot{\mathbf{q}} \tag{2.52}$$

into (2.49) and rearranging terms yields implicit equation with respect to $\delta\ddot{\mathbf{q}}$

$$[\mathbf{M} + \Delta t\gamma\mathbf{C}]\,\delta\ddot{\mathbf{q}} = \mathbf{p}_{n+1} - \mathbf{b}_{n+1}^{(i)} - \mathbf{c}_{n+1}^{(i)} - \mathbf{r}(\mathbf{q}_{n+1}^{(i)} + (\Delta t)^2\beta\delta\ddot{\mathbf{q}}). \tag{2.53}$$

The correction of $\delta\ddot{\mathbf{q}}$ is found using method of simple iteration

$$\delta\ddot{\mathbf{q}} = [\mathbf{M} + \Delta t\gamma\mathbf{C}]^{-1}\left(\mathbf{p}_{n+1} - \mathbf{b}_{n+1}^{(i)} - \mathbf{c}_{n+1}^{(i)} - \mathbf{r}(\mathbf{q}_{n+1}^{(i)})\right). \tag{2.54}$$

It is clear that if $\mathbf{M}$ and $\mathbf{C} = \eta\mathbf{M}$ are by assumption pseudo-diagonal substantial efficiency of computation is gained. The so designed integration scheme is fast and efficient in the context of the wave propagation analysis.

The equation (2.54) is solved in the iterative way until the equilibrium condition becomes satisfied

$$\mathbf{j}_{n+1}^{(i+1)} = \mathbf{p}_{n+1} - \mathbf{b}_{n+1}^{(i+1)} - \mathbf{c}_{n+1}^{(i+1)} - \mathbf{r}(\mathbf{q}_{n+1}^{(i+1)}) \;\rightarrow\; \mathbf{0}. \tag{2.55}$$

The iterations are terminated if convergence is achieved. Since in view of (2.54), the equation (2.55) is equivalent to $\delta\ddot{\mathbf{q}} \rightarrow \mathbf{0}$ the convergence is assessed using the relative convergence criteria

$$\frac{\|\delta\ddot{\mathbf{q}}\|}{\|\ddot{\mathbf{q}}_{n+1}^{(i+1)} - \ddot{\mathbf{q}}_n\|} < \varepsilon_1, \quad \max_k \frac{|\delta\ddot{q}_k|}{\left|\ddot{q}_{kn+1}^{(i+1)} - \ddot{q}_{kn}\right|} < \varepsilon_2, \tag{2.56}$$

where $\|.\|$ is Euclidean norm of a vector and ε_1 and ε_2 are a priori assumed. Once (2.54) is solved the remaining state variables are updated through relations (2.50)–(2.52).

3. N

3.1. G

The possibility of damage detection in spatial truss is studied on the example of the star dome presented, e.g., in [22]. The geometry of the dome (Fig. 4) has been taken from [22] while the remaining properties has been adopted as: modulus of elasticity $E = 210$ GPa mass density $\rho = 7850$ kg/m^3, element area $A = 2\times10^{-7}$ m^2. The damping parameter η in Eq. (2.39) equals 200 1/s. The value of the damping parameter was chosen based on experimental investigations carried out on the simple rod.

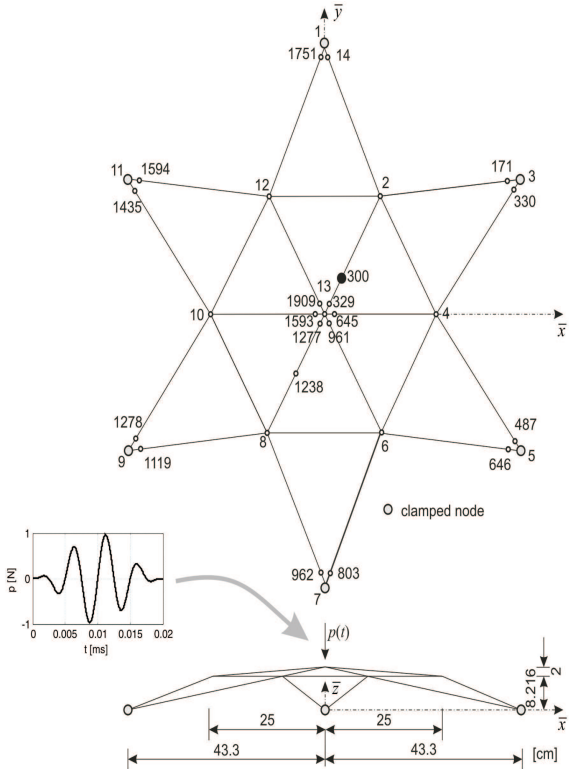

Fig. 4. Star dome structure, top and front view, geometry and load.
Rys. 4. Konstrukcja kopuły w kształcie gwiazdy, rzut z góry i boku, geometria i obciążenie

The elastic wave actuator is located at the top of the dome. As an excitation the sinusoidal signal of amplitude 1 N and of frequency 200 kHz modulated by the Hanning window was applied. The load has been placed at the node 13 of the structure model along global $\bar{z}$ axis. The total time of load action is $t = 0.02$ ms. Two cases are considered: in the first case a structure is ideal (case 1) while in the second case the

structure has the additional mass (case 2). The additional mass is equal 2% of the total mass of the truss girder. The time step was assumed as 10^{-8} s.

3.2. S

Based on experimental and numerical simulations performed for a simple rod it has been concluded, that only the GLL distribution of nodes in both geometric coordinates and the natural coordinates guaranties the appropriate modelling of wave propagation. Both the GLL and Gauss integration rule can be used, however the GLL integration rule is more effective. The minimum number of nodes for proper response modelling is about 7 nodes per wavelength. Based on the above results the spectral element with 81 GLL distributed nodes in both geometric and natural coordinates is applied to the numerical model of the 3D truss.

To assess the correctness of the numerical model the acceleration of all the nodes in the vicinity of the star dome top were plotted in Fig. 5a. It is visible, that all acceleration signals are the same as they should be due to the geometrical symmetry of the structure. The similar comparison for the nodal accelerations in the vicinity of the fixed supports is illustrated in Fig. 5b.

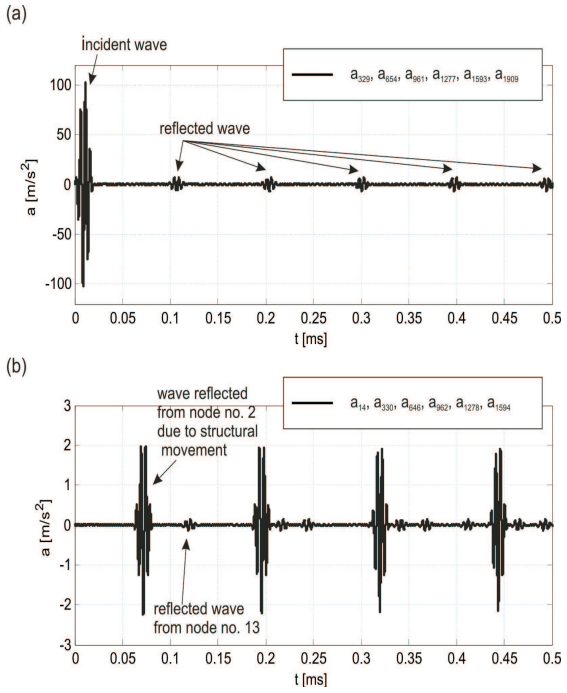

Fig. 5. Acceleration history: a) nodes near the top, b) nodes near the support.
Rys. 5. Sygnały czasowe przyspieszeń: (a) węzły w sąsiedztwie wierzchołka kopuły, (b) węzły w pobliżu podpory

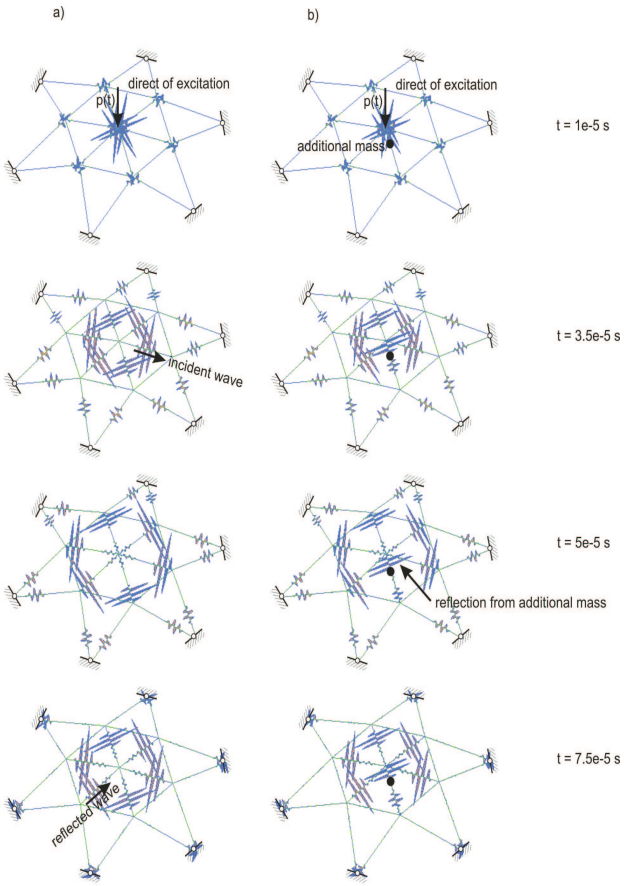

Fig. 6. Animation of wave propagation in star dome: a) ideal structure, b) structure with additional mass.
Rys. 6. Animacja propagacji fal w kopule: (a) konstrukcja bez dodatkowej masy, (b) konstrukcja z dodatkową masą

Figure 6a illustrates the snapshots from the animation depicting the movement of the waves for the structure without additional mass. Animation was performed using GiD postprocessor [22]. The wave signal excitation imposed at node 13 in the vertical direction causes structural movement all structural nodes in the time instance $t = 0$ ms. The first time instance in Fig. 6 has been selected as 0.01 ms, when the front of the wave starts propagating. In the time instance $t = 0.035$ ms wave propagates through the all structural elements. In the next selected time instance $t = 0.05$ the waves reflect from the nodes 2, 4, 6, 8 10 and 12. In the last time instances $t = 0.075$ ms, the reflected waves are visible.

The case 2 concerns the truss with additional mass. The additional mass was added at the node no. 300, in the distance of 7.77 cm from the node 13 (Fig. 4). In Fig. 6b animation of propagating waves are illustrated.

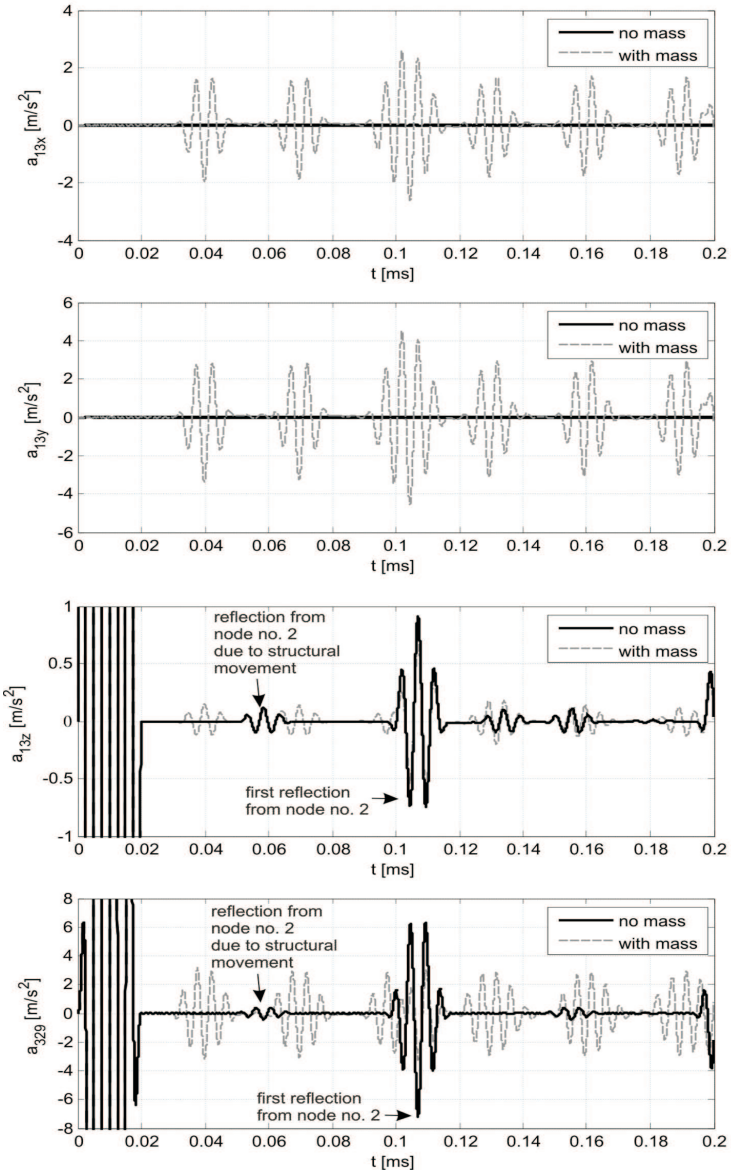

Fig. 7. Acceleration at nodes 13 and 329 for the star dome without additional mass and with additional mass.

Rys. 7. Sygnał przyspieszenia w węzłach 13 i 329 dla konstrukcji bez dodatkowej masy i z dodatkową masą

The comparison of the acceleration signals for the node 13 and 329 is shown in Fig. 7. The accelerations of node 13 in both $\bar{x}$ and $\bar{y}$ direction are close to zero for the case without the additional mass. However, when the mass is added, the reflections appear. In the acceleration of node 13 and 329 there are visible peaks corresponding to the wave reflecting from the truss nodes as well as from the additional mass in the horizontal acceleration response at the node 2. The time of reflection from the additional mass is found to be 0.0297 ms. The knowledge of the reflecting time and the wave speed enables to estimate the localization of the additional mass as 7.68 cm.

4. C

In this paper the formulation of elastic wave propagation in spatial steel truss is presented. The numerical simulations are conducted on the star dome example. The modelling of the star dome was performed by the spectral element method with the Lobbato integration rule. 81-node elements have been applied. Use of Gauss-Legendre-Lobatto (GLL) nodes is necessary to avoid the Runge effect. Despite of using the Lobatto integration rule, the mass matrix is not diagonal. The mass matrix losses the diagonal form in the process of transformation from local to global coordinate system. However, it remains pseudo diagonal and integration of the equations of wave propagation can be efficiently conducted.

The numerical simulations have been performed for an ideal truss as well as for the truss with singularity points imposed by the additional mass. The location of additional mass can be estimated by analysis of the travelling times of the incident and reflected waves.

A

The authors are grateful to the support of the Polish Ministry of Science and Higher Education via Grant no. N506 065 31/3149 entitled: “Multilevel damage detection system in engineering structures”.

Magdalena Rucka would also thank the Foundation for Polish Science for being granted the Scholarschip for Young Scientists in the year 2008.

R

1. M.J.S L , D.N. A , P. C , Defect detection in pipes using guided waves, Ultrasonics, **36**, 147–154, 1998.
2. R. P. D , P. C , M. J. S. L , *The potential of guided waves for monitoring large areas of metallic aircraft fuselage structures*, Journal of Nondestructive Evaluation, **20**, 29–46, 2001.
3. F. M , L.J. J , J. Q , *Modeling elastic wave propagation in waveguides with the finite element method*, NDT&E International, **32**, 225–234, 1999.

4. L. G ˆ, *Computation of propagative waves in free rail using finite element technique*, Journal of Sound and Vibration, **185**, 531–543, 1995.
5. J.F. D , *Wave propagation in structures: spectral analysis using fast discrete Fourier transforms*, second ed. Springer-Verlag, New York 1997.
6. M. P , M. K , *Analysis of longitudinal wave propagation in a cracked rod by the spectral element method*, Computers & Structures, **80**, 1809–1816, 2002.
7. M. K , M. P , W. O , *The dynamic analysis of a cracked Timoshenko beam by the spectral element method*, Journal of Sound and Vibration, **264**, 1139–1153, 2003.
8. M. K , M. P , W. O , *Wave propagation in plate structures for crack detection*, Finite Elements in Analysis and Design, **40**, 991–1004, 2004.
9. S. G , A. C , D. R. M , *Spectral finite element method: wave propagation, diagnostics and control in anisotropic and inhomogeneous structures*, Springer-Verlag, London 2008.
10. T. P , *A spectral element method for fluid dynamics: laminar flow in a channel expansion*, Journal of Computational Physics, **54**, 468–488, 1984.
11. C. C , M. Y. H , A. Q , T. A. Z , *Spectral Methods in Fluid Dynamics*, Springer Verlag, Berlin, Heidelberg 1998.
12. P. K , M. K , W. O , *Wave propagation modelling in 1D structures using spectral finite elements*, Journal of Sound and Vibration, **300**, 88–100, 2007.
13. P. K , A. Ż , M. K , W. O , *Modelling of wave propagation modelling in composite plates using the time domain spectral element method*, Journal of Sound and Vibration, **302**, 728–745, 2007.
14. A. Ż , M. K , W. O , *Propagation of in-plane wave in an isotropic panel with a crack*, Finite Elements in Analysis and Design, **42**, 929–941, 2006.
15. A. Ż , M. K , W. O , *Propagation of elastic waves in Shell-like structures*, Proceedings of the Fourth European Workshop on Structural Health Monitoring, 533–539, 2008.
16. http://www.mathworks.com/matlabcentral/fileexchange
17. W.H. P , S.A. T , W.T. V , B.P, F , *Numerical recipes in Fortran 90: the art of parallel scientific computing*, Cambridge University Press 1999.
18. C. P , *Introduction to Finite and Spectral Element Methods using MATLAB®*, Chapman & Hall/CRC, 2005.
19. T.J.R. H , *The finite element method: linear static and dynamic finite element analysis*, Dover 2000.
20. N.N. N , *A method of computation for structural dynamics*, Proc ASCE, J. Engng. Mech. Div., **85**, (EM3),67–94, 1959.
21. M. G , F.A.R. G , W.S. V , H.B. C , *Nonlinear positional formulation for space truss analysis*, Finite Elements in Analysis and Design, **42**, 1079–1086, 2006.
22. http://gid.cimne.upc.es/

SFORMUŁOWANIE WIELOWĘZŁOWEGO KRATOWEGO ELEMENTU SPEKTRALNEGO DO WYKRYWANIA USZKODZEŃ W STRUKTURACH PRZESTRZENNYCH ZA POMOCĄ FAL SPRĘŻYSTYCH

S t r e s z c z e n i e

W pracy przedstawiono sformułowanie wielowęzłowego elementu spektralnego oraz odpowiedniego schematu całkowania ukierunkowanego na problem propagacji fal w kratownicach przestrzennych o dowolnej

geometrii. Zaproponowane podejście nie ogranicza liczby węzłów w elemencie kratowym. Porównawcze rozwiązania numeryczne przeprowadzono dla konstrukcji idealnej (w stanie nieuszkodzonym) oraz dla konstrukcji z miejscową nieregularnością w formie dodatkowej masy. Zadaniem odbieranych w punkcie pomiarowym sygnałów czasowych przyspieszeń fal sprężystych jest wykrycie i zlokalizowanie pozycji dodatkowej masy. W pracy przeprowadzono dyskusję nad możliwością detekcji uszkodzeń w konstrukcjach kratowych na podstawie analizy fal sprężystych.

Remarks on the paper should be sent to the Editorial Office no later than June 30, 2009

Received August 11, 2008
revised version
February 16, 2009